Near-surface ocean temperature

B. Ward

Department of Applied Ocean Physics and Engineering, Woods Hole Oceanographic Institution, Woods Hole, Massachusetts, USA

Received 14 September 2004; revised 31 August 2005; accepted 26 September 2005; published 11 February 2006.

[1] The first open ocean deployment of the Skin Depth Experimental Profiler (SkinDeEP) was from the R/V *Melville* in the Gulf of California during the Marine Optical Characterization Experiment (MOCE-5). SkinDeEP is an autonomous, vertical profiler for the upper few meters of the ocean. During MOCE-5, SkinDeEP was deployed on ten separate occasions, and profiles were made at intervals of approximately 1 min each. A total of 976 profiles was acquired during the cruise. The ocean skin temperatures were measured by the Marine Atmosphere Emitted Radiance Interferometer (M-AERI), an infrared spectroradiometer. Typical meteorological conditions were of low winds and high insolation. The data set provided captures the near-surface temperature structure that decouples the skin layer from the conventional in situ bulk sea surface temperature (SST) measurements made at a depth of a few meters. Data from SkinDeEP showed strong diurnal warming within the upper few meters, with one extreme case of 4.6 K. There were large discrepancies when computing the skin-bulk temperature difference with bulk temperatures at different depths. Results also show the strong dependency of the SST on air-sea heat flux estimates, with warm-layer errors of almost 60 Wm^{-2} associated with intense stratification. This indicates the importance of the inclusion of the skin temperature for accurate calculation of latent, sensible, and net longwave heat fluxes.

Citation: Ward, B. (2006), Near-surface ocean temperature, *J. Geophys. Res.*, *111*, C02004, doi:10.1029/2004JC002689.

1. Introduction

[2] Sea surface temperature (SST) is one of the key parameters governing the air-sea exchange of heat [*Fairall et al.*, 1996a] and gas [*Ward et al.*, 2004b]. Heat flux estimates with accuracies of 10 Wm^{-2} are required to reduce errors in atmospheric models. These estimates are extremely sensitive to SST variability, especially in lower latitudes [*Fairall et al.*, 1996b].

[3] Historically, sea surface temperature was ascribed to observations made from ships by measuring the bulk water temperature within the mixed water column, usually somewhere within the top 10 m and often at an arbitrary and imprecisely known depth, using bucket thermometers or the ship's cooling water intake. *Donlon et al.* [2002] classifies the vertical structure of SST according to the depth of measurement (Figure 1). The skin SST (T_{skin}), is essentially the temperature measured by a radiometer. The subskin SST ($T_{subskin}$) is representative of the SST at the bottom of the conductive boundary layer. The subsurface SST (T_{depth}) represents the temperature within the water column beneath the $T_{subskin}$, and is most often the only available SST.

[4] Bulk formula heat flux calculations require SST for the determination of sensible and latent turbulent heat fluxes. It is also needed to calculate upwelling longwave emission. The most appropriate SST for these formulae is the skin temperature, as this is the temperature of water which is in direct contact with the atmosphere [*Fairall et al.*, 1996b]. When radiometric measurements during field campaigns are unavailable, a model is required to calculate T_{skin} from oceanographic and meteorological measurements. The model in the work of *Fairall et al.* [1996a] takes into account both cool-skin and warm-layer effects:

$$T_{skin} = T_{depth}(z_r) + \Delta T_w(z_r) + \Delta T_c, \tag{1}$$

$$\Delta T_c = T_{skin} - T_{subskin}, \tag{2}$$

$$\Delta T_w = T_{subskin} - T_{depth}, \tag{3}$$

where $\Delta T_w(z_r)$ is the warm-layer correction resulting from the measurement $T_{depth}(z_r)$ at some reference depth z_r, and ΔT_c is the cool-skin correction.

[5] Figure 1 schematically represents the model in equation (1). There is a linear temperature gradient between T_{skin} and $T_{subskin}$, as the conductive boundary layer is embedded in the viscous sublayer, and molecular processes dominate. This figure also shows a SkinDeEP profile, which was acquired during station 10 of this cruise at 1139 local solar time (LST). There is a ΔT_w of 2.5 K, and a ΔT_c of -0.6 K, which adequately represent oceanic conditions under low wind speeds (*Fairall et al.* [1996a] suggests typical values of 3 K for ΔT_w and -0.1 to -0.5 K for ΔT_c). Under nighttime conditions, or when the water column is well-mixed, $T_{depth} \cong T_{subskin}$ and ΔT_w is zero. However, under

0148-0227/06/2004JC002689$09.00

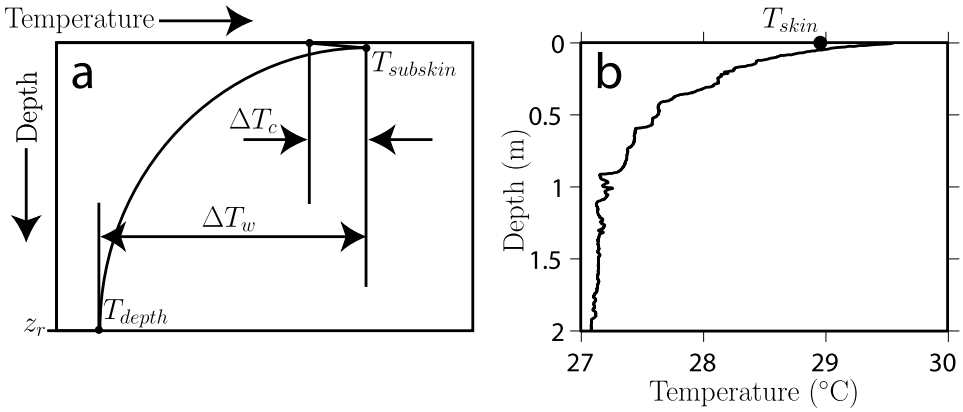

Figure 1. (a) Schematic showing the vertical temperature structure in the upper few meters of the ocean under conditions of diurnal warming. This is a schematic representation of the model from *Fairall et al.* [1996a], expressed in equation (1). (b) Actual profile taken in the upper 2 m with SkinDeEP during station 10 (see section 3.6). The solid circle indicates the radiometric temperature measurement of T_{skin} from the M-AERI.

conditions of near-surface stratification, ΔT_w becomes very dependent on the reference depth z_r.

[6] This paper presents measurements of diurnal warming taken by the SkinDeEP profiler, an autonomous, vertical, temperature profile. Profiles were made at intervals of about 1 min over the uppermost few meters, with vertical spatial resolutions of O(1 mm). The combination of high vertical resolution and rapid profile intervals provided near-surface temperature measurements with unprecedented detail. The M-AERI spectroradiometer also provided high accuracy skin temperature measurements. A brief description of the cruise and available measurements are presented in section 2. Section 3 presents the results from each of the 10 stations. In section 4, these results are discussed in relation to the cool-skin and warm-layer temperature differences and the errors in heat flux calculations from the vertical variability in SST. Our conclusions are provided in section 5.

2. Cruise Data

[7] The MOCE-5 cruise was in the area of Baja California, both in the Pacific Ocean to the west of the peninsula and in the Gulf of California (Figure 2). The cruise was conducted in October 1999.

[8] High-resolution temperature measurements were provided by SkinDeEP, an autonomous vertical profiler. A thorough description of the instrument is provided by *Ward et al.* [2004c]. Some preliminary results from this cruise were also presented by *Minnett and Ward* [2000], of which see Figure 2 for a schematic of the MOCE-5 version of SkinDeEP *Ward and Minnett* [2002]. SkinDeEP was deployed on 10 separate occasions both inside and outside the Gulf (Figure 2). The profiler was dropped from the stern of the ship, and was attached to a surface spar buoy with a 50-m neutrally buoyant line. During SkinDeEP deployments, the instrument drifted while the ship remained on station to conduct other operations.

[9] Once deployed, SkinDeEP made profiles continuously at intervals of one minute, with the longest deployment being 3 hours. There are a total of 976 profiles available from this cruise (Table 1), during which temperature and depth were the only parameters measured by SkinDeEP. Data were recorded from within the water column to the surface, and only during the ascent. The time response of the temperature sensor on SkinDeEP (a Thermometrics FP07) is 7 ms (although this has a velocity dependence, where the time response will vary as $-1/2$ power of the velocity [*Gregg and Meagher*, 1980]). With a nominal rise velocity $\sim$0.5 ms^{-1}, the spatial resolution of SkinDeEP is better than 3 mm, and so it is assumed that the surface measurement from SkinDeEP provides $T_{subskin}$ with negligible error.

[10] Continuous skin temperature was provided by M-AERI, a passive infrared radiometric interferometer which makes radiance measurements in the 500–3000 cm^{-1} wave number range with a resolution of 0.5 cm^{-1}. A rotating gold-plated mirror allows for both sea and sky views at complementary angles to nadir and zenith. Realtime calibration is

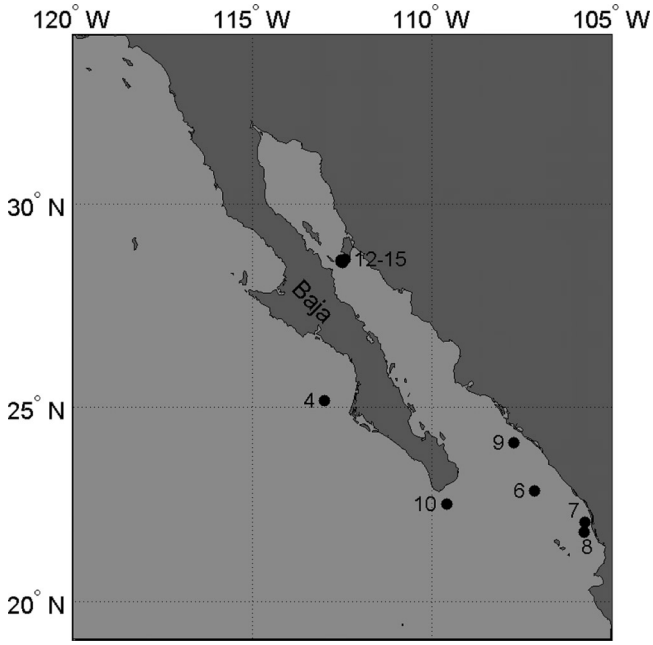

Figure 2. Map of the Gulf of California showing the positions of each of the SkinDeEP deployments and corresponding station numbers.

Table 1. Station Number, Yearday, Times (Local Solar Time), Positions, and Number of Profiles for Each of the Ten SkinDeEP Deployments[a]

Station Number	Yearday	Time, LST	Latitude	Longitude	Number of Profiles
4	277	1059–1324	25°09.49N	112°59.52W	120
6	279	1536–1603	22°52.04N	107°10.02W	27
7	280	1401–1524	22°03.40N	105°46.06W	74
8	281	1402–1540	21°49.06N	105°47.20W	89
9	282	1311–1533	24°06.06N	107°44.29W	112
10	283	1112–1413	22°31.48N	109°35.43W	161
12	285	1422–1637	28°38.51N	112°25.16W	114
13	286	1444–1634	28°38.06N	112°32.28W	95
14	287	0615–0744	28°36.15N	112°32.04W	78
15	287	1801–1948	28°34.57N	112°29.30W	106

[a]Latitude and longitude positions were taken from the ship's navigational data. Station numbers were derived from the experiment cruise log.

accomplished by viewing two internal blackbody cavities, one at 60°C and one at ambient temperature. Measurements are integrated over several tens of seconds to obtain a satisfactory signal-to-noise ratio, and a typical measurement cycle including two view angles of the atmosphere, one to the ocean, and calibration, takes about 12 min. The accuracy of the derived SSTs from M-AERI is better than 0.05 K. A more detailed description of M-AERI can be found in the work of *Minnett et al.* [2001].

[11] The conditions encountered during the 10 deployments of SkinDeEP are presented in Figure 3. The downwelling shortwave radiation reached over 800 Wm^{-2} on every day except for YD 281. On days 277 and 278 it peaked at over 900 Wm^{-2}. The wind speed never exceeded 10 ms^{-1}, and during some of the deployments, it was below 2 ms^{-1} (the mean wind speed for the period shown in Figure 3 was 3.5 ± 1.8 ms^{-1}).

[12] The heat fluxes were calculated using the bulk aerodynamic equations with transfer coefficients given by *Fairall et al.* [1996a]. These coefficients were derived from

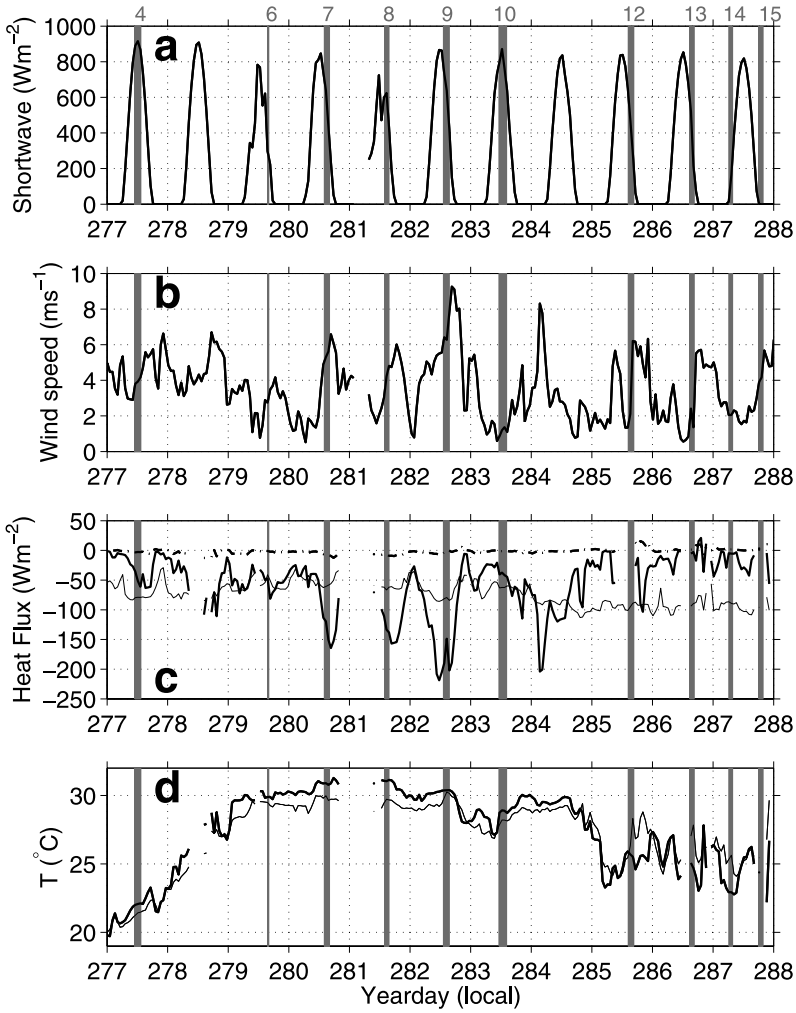

Figure 3. Time series of some relevant parameters during the MOCE-5 cruise. From the top: (a) Downwelling shortwave radiation. (b) Wind speed. (c) Latent (thick lines), sensible (dashed lines), and net longwave (thin lines) heat fluxes. (d) Skin temperature (thick) and air temperature (thin lines), both from M-AERI. The vertical bars represent the time when SkinDeEP was deployed, with station numbers indicated. All data were averaged over 60 min.

Table 2. Mean ($\overline{T}$) and Standard Deviation ($\widetilde{T}$) of $T_{subskin}$ (SkinDeEP), T_{5m} (SkinDeEP), and T_{skin} (M−AERI) for Each Station

Station	$\overline{T}_{subskin}$, °C	$\widetilde{T}_{subskin}$, °C	$\overline{T}_{5m}$, °C	$\widetilde{T}_{5m}$, °C	$\overline{T}_{skin}$, °C	$\widetilde{T}_{skin}$, °C
4	22.07	0.19	21.65	0.04	22.09	0.04
6	29.94	0.04	29.70	0.01	29.91	0.08
7	31.13	0.03	30.64	0.01	30.88	0.06
8	31.47	0.05	30.87	0.11	31.06	0.06
9	30.55	0.02	30.54	0.02	30.38	0.06
10	29.16	0.26	27.03	0.01	28.85	0.18
12	25.66	0.21	24.33	0.34	25.67	0.27
13	25.47	0.35	22.40	1.20	24.87	0.26
14	22.98	0.03	22.96	0.01	22.88	0.08
15	24.75	0.12	24.28	0.22	23.88	0.36

measurements in the Tropical Western Pacific and are appropriate for application to these conditions. TOGA-COARE code version 2.0 was used for the heat flux computations [*Pawlowicz et al.*, 2001]. M-AERI sea and air temperatures were used in the calculation of the fluxes. The cooling at the surface (Figure 3) is dominated by the latent heat flux, which reached a maximum of −228 Wm^{-2} on YD 282, when the highest winds were encountered. The sensible heat flux is relatively low, due to the small air-water temperature difference throughout the cruise. Toward the end of the cruise, the net longwave dominated the heat loss at the surface.

[13] The range in SST (Figure 3) was from about 20–30°C, reaching a maximum at stations 6 to 9 south of the Gulf. Air-sea temperature differences were negative until about day 285, when measurements were conducted toward the Gulf's midriff (Figure 2). Here the proximity to the land appears to have influenced the air-water temperature difference.

3. SkinDeEP Measurements: Case Studies

[14] Table 2 presents mean and standard deviation values of SkinDeEP surface data ($T_{subskin}$), SkinDeEP data at a depth of 5 m (T_{5m}), and the skin temperature derived from the M-AERI (T_{skin}).

[15] Table 3 presents mean values of sensible (Q_s), latent (Q_e), net longwave ($Q_{lw}\Updownarrow$) and total heat loss (Q) at the surface, computed for this data set. Also presented in Table 3 are measured downwelling shortwave radiation ($Q_{sw}\Downarrow$) and wind speed (u). For each station, the data were averaged over 10-min intervals, and the heat flux components were calculated using T_{skin}, $T_{subskin}$, and T_{5m}. The bulk formula for the heat flux components are:

$$Q_s = \rho_a c_p C_s u(T_a - \mathbf{T}), \tag{4}$$

$$Q_e = \rho_a L_e C_e u(q_a - \mathbf{q_s}), \tag{5}$$

$$Q_{lw}\Updownarrow = Q_{lw}\Downarrow - \epsilon\sigma\mathbf{T}^4, \tag{6}$$

$$Q = Q_s + Q_e + Q_{lw}\Updownarrow, \tag{7}$$

where $Q_{lw}\Downarrow$ is the measured downwelling longwave radiative flux, ρ_a is air density, c_p is the specific heat capacity of air, C_s is the Dalton number (sensible heat transfer coefficient), $\mathbf{T}$ is the sea surface temperature, T_a is the air temperature, L_e is the latent heat of vaporization, C_e is the Stanton number (transfer coefficient for latent heat), $\mathbf{q_s}$ is the interfacial value of the specific humidity, q_a is the atmospheric specific humidity, ϵ is the sea surface emissivity (∼0.98), and σ is the Stefan–Boltzmann constant (5.67×10^{-8} JK^{-4} m^{-2} s^{-1}). SST-dependent parameters in equation (2) have a bold font.

[16] The main display of data is presented in Figures 4a to 4j. All times shown are in LST, which defines local noon as the time when the Sun is at its meridian. Graph I shows temperature-depth plots of the SkinDeEP profiles. Wind speed and downwelling shortwave radiation are shown in graph II. Cool-skin and warm-layer temperature differences (Δ_c and ΔT_w, respectively) are presented in graph III. Also shown is ΔT_{cw}, defined as: $\Delta T_{cw} = T_{skin} - T_{depth}$; this is the skin-bulk temperature difference which is most often available during shipboard campaigns (i.e., with a typical ship intake depth of about 5 m). The reference depth z_r in (1) is 5 m. Graph IV shows the discrepancies in the heat flux associated with these temperature differences:

$$\Delta Q_c = Q(T_{skin}) - Q(T_{subskin}), \tag{8}$$

$$\Delta Q_w = Q(T_{subskin}) - Q\big(T_{depth}\big), \tag{9}$$

$$\Delta Q_{cw} = Q(T_{skin}) - Q\big(T_{depth}\big). \tag{10}$$

A negative heat flux error value indicates an underestimation of the heat flux.

3.1. Station 4

[17] Figure 4a shows data from the first day of measurements made by SkinDeEP. The time of the deployment was

Table 3. Mean Latent (Q_e), Sensible (Q_s), and Net Longwave ($Q_{lw}\Updownarrow$) Computed With $T_{subskin}$ (SkinDeEP), T_{5m} (SkinDeEP), and T_{skin} (M−AERI)[a]

Station Number	4	6	7	8	9	10	12	13	14	15
$\overline{Q_e}(T_{subskin})$ (Wm^{-2})	−47.10	−38.62	−125.30	−135.27	−165.70	−42.26	−25.10	−14.24	−5.06	−13.33
$\overline{Q_e}(T_{5m})$ (Wm^{-2})	−39.34	−34.50	−107.39	−116.89	−165.17	−6.01	−6.37	0.20	−5.04	−6.92
$\overline{Q_e}(T_{skin})$ (Wm^{-2})	−47.50	−38.33	−116.19	−122.23	−157.80	−38.33	−25.47	−5.34	−4.95	−3.35
$\overline{Q_s}(T_{subskin})$ (Wm^{-2})	−1.96	−0.12	−6.27	−8.56	−0.06	−1.74	4.41	2.07	1.64	4.31
$\overline{Q_s}(T_{5m})$ (Wm^{-2})	0.16	0.61	−2.80	−4.93	0.04	0.60	3.27	3.35	1.64	4.67
$\overline{Q_s}(T_{skin})$ (Wm^{-2})	−2.10	−0.06	−4.49	−5.98	1.37	−1.03	4.37	1.70	1.68	4.85
$\overline{Q_{lw}\Updownarrow}(T_{subskin})$ (Wm^{-2})	−79.05	−40.05	−62.26	−68.01	−82.27	−64.60	−93.35	−94.42	−87.86	−97.32
$\overline{Q_{lw}\Updownarrow}(T_{5m})$ (Wm^{-2})	−76.69	−38.61	−59.18	−64.26	−82.20	−51.56	−85.44	−75.61	−87.81	−94.57
$\overline{Q_{lw}\Updownarrow}(T_{skin})$ (Wm^{-2})	−79.23	−39.90	−60.69	−65.35	−81.17	−62.66	−93.38	−91.23	−87.34	−92.45
$\overline{Q_{sw}\Downarrow}$($Wm^{-2}$)	902	243	629	605	653	795	430	473	102	0
$\overline{u}$ (ms^{-1})	4.0	2.5	5.3	4.3	6.6	1.1	3.5	2.4	2.0	4.0

[a]Also shown is the mean downwelling shortwave radiation ($Q_{sw}\Downarrow$) and wind speed (u).

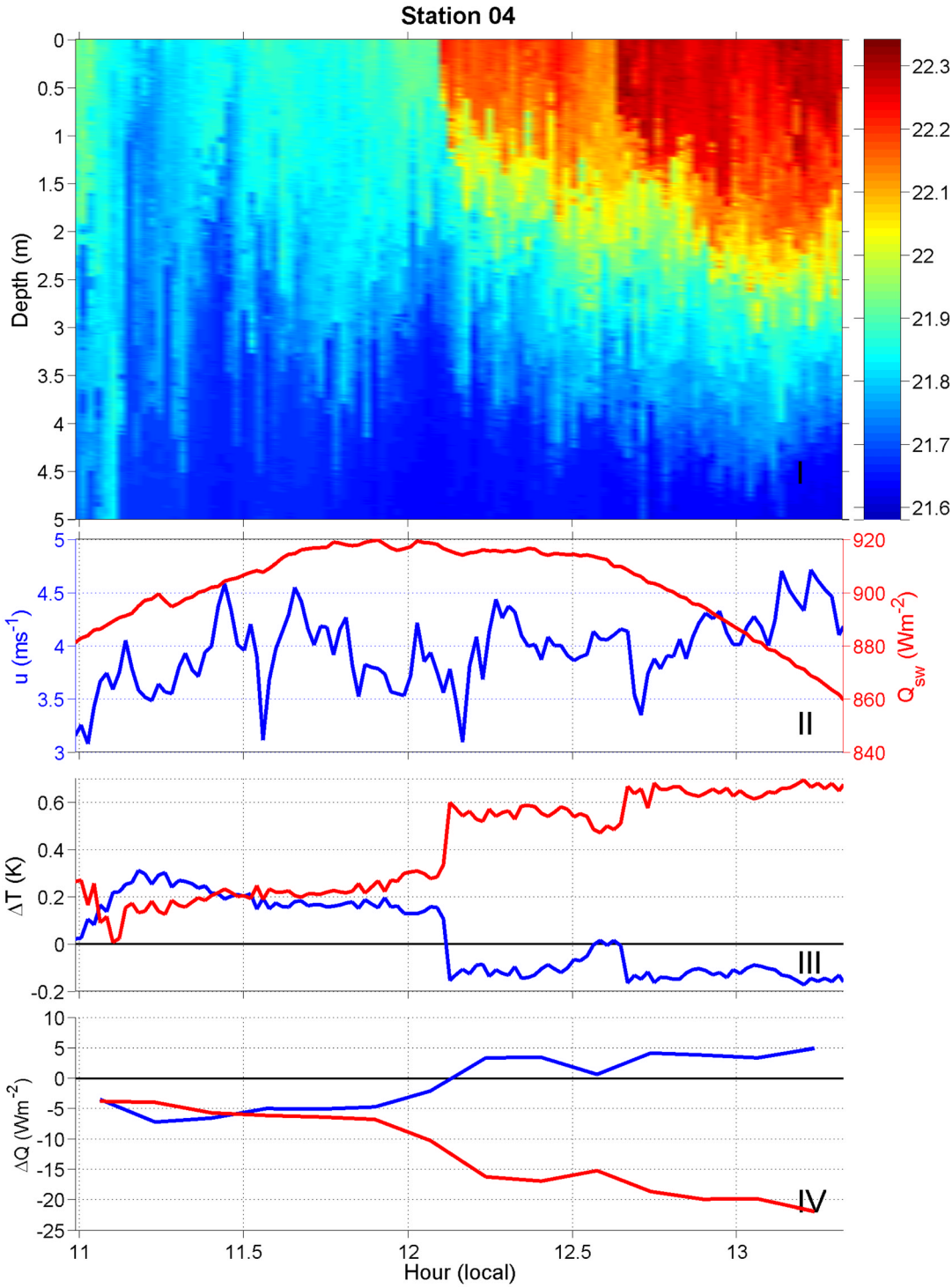

Figure 4a. Temperature-depth measurements from SkinDeEP (graph I). Wind speed (u) and downwelling shortwave radiation (Q_{sw}) (graph II). Temperature differences: ΔT_c (blue), ΔT_w (red), and ΔT_{cw} (green) (graph III). Heat loss errors: ΔQ_c (blue), ΔQ_w (red), and ΔQ_{cw} (green) (graph IV).

just before 11:00 and lasted until about 14:00. The wind speed during this period reached a maximum of 4.7 ms^{-1}, and the maximum shortwave radiation was 920 Wm^{-2}.

[18] The radiometric temperature T_{skin} had a mean value of 22.1°C, with little variation (Table 2). $T_{subskin}$ was approximately the same as T_{5m} until just after 12:00, when a sharp gradient of 0.3 K was encountered, the most likely cause being that SkinDeEP passed through a weak thermal front. At this point, ΔT_c changed sign from positive to negative. There was also a sharp increase in ΔT_w from about 0.3 K to 0.6 K. This was not apparent in ΔT_{cw} as neither T_{skin} nor T_{5m} experienced this abrupt change.

[19] The largest heat flux error was derived from the latent flux. The uncertainties from both the sensible and longwave

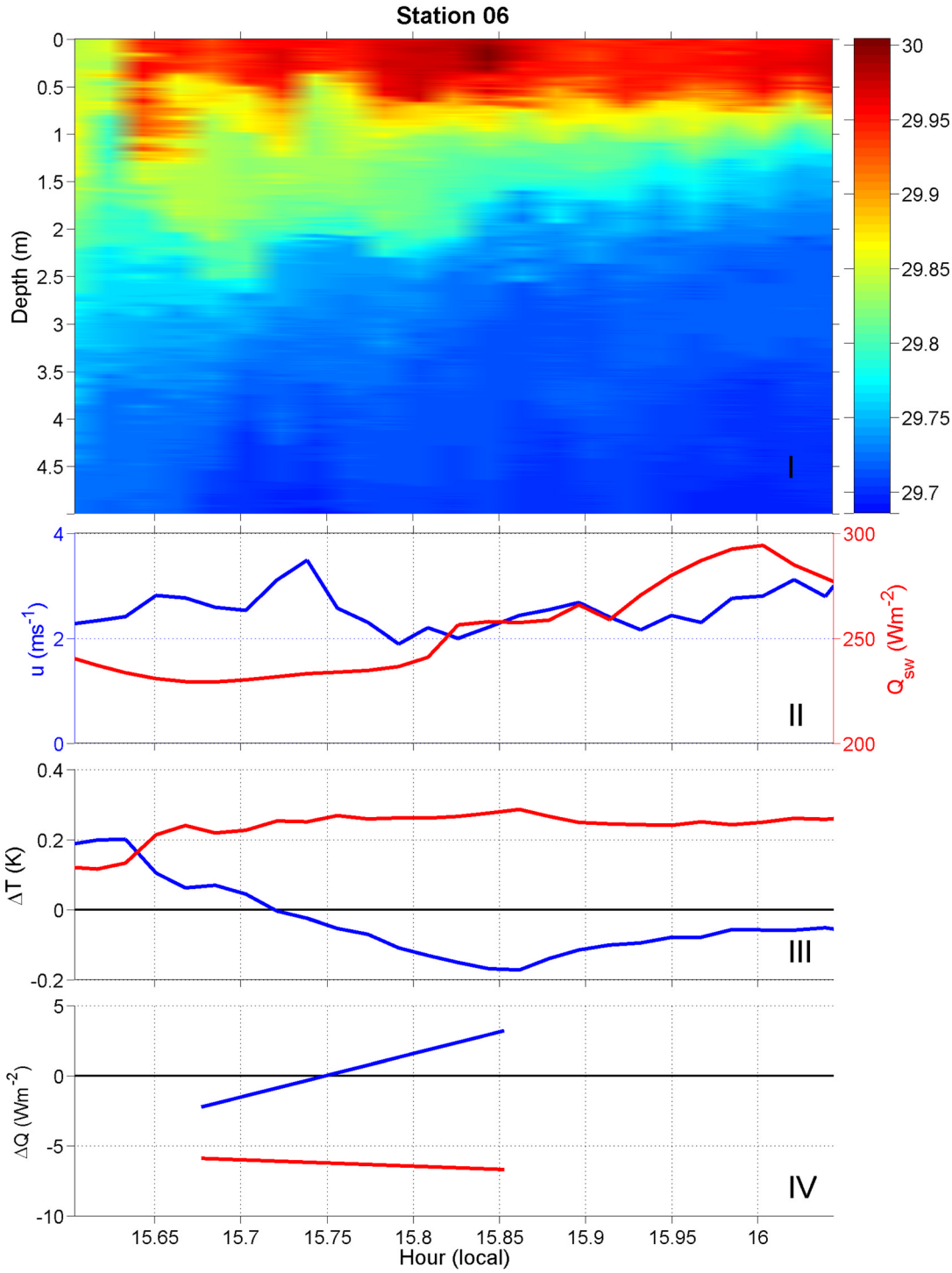

Figure 4b. Same as Figure 4a.

fluxes were much smaller than those in the latent heat flux, even though the largest absolute heat flux component at the surface was the net longwave (Table 3). The total mean heat loss errors were: -0.7 ± 4.5, -12.2 ± 6.7, and -13 ± 2.6 Wm^{-2} for ΔQ_c, ΔQ_w, and ΔQ_{cw}, respectively.

3.2. Station 6

[20] The deployment at station 6 (Figure 4b) was situated just outside the mouth of the Gulf (Figure 2), with an average water temperature of 29.7°C over the depth range sampled by SkinDeEP. This was the shortest deployment of SkinDeEP, lasting only 30 min from about 15:30 to 16:00. The average wind speed was 2.5 ms^{-1}, but with a maximum of 3.5 ms^{-1}. The mean downwelling shortwave radiation was 253 Wm^{-2} during the deployment, but had reached a maximum of 840 Wm^{-2} at noon, some hours before the measurements occurred. The profiler data showed a warm-layer in the upper 2 m, and stratification was further enhanced in the top meter.

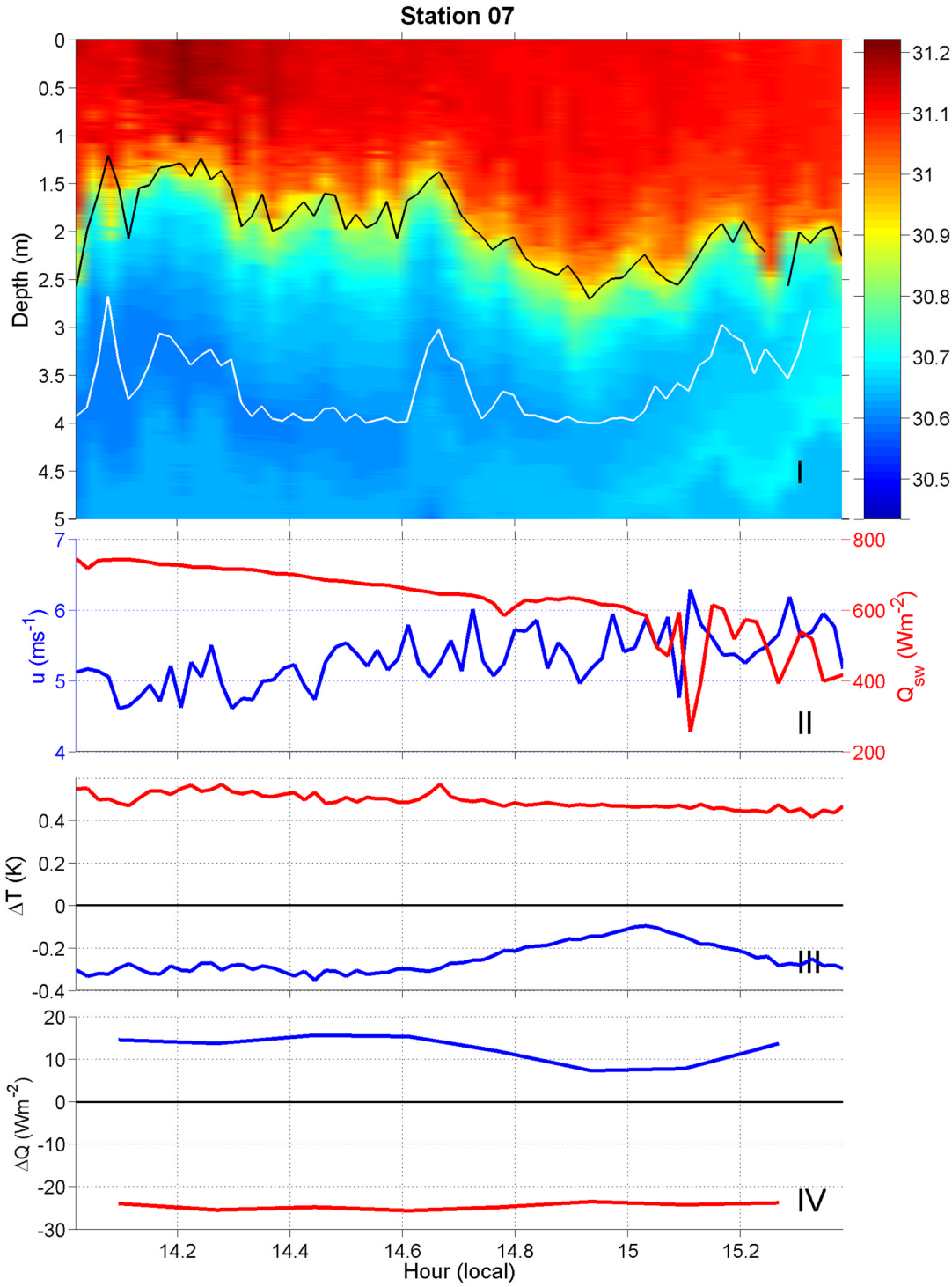

Figure 4c. Same as Figure 4a.

[21] $T_{subskin}$ increased just after deployment from 29.8 to about 30°C, and remained quite constant through to the end of the deployment. There was an almost constant offset between ΔT_c and ΔT_{cw}, with mean values of −0.03 and +0.2 K, respectively. ΔT_w had a mean value of +0.24 K.

[22] The major source of heat loss to the atmosphere was from the latent heat flux, which was marginally greater than the longwave; the sensible heat flux was negligible during this station (Table 3). ΔQ_{cw} had the largest error with a maximum of −8.1 Wm^{-2}, followed by ΔT_w at −6.6 Wm^{-2}, and ΔT_c with +3.2 Wm^{-2}.

3.3. Station 7

[23] Station 7 (Figure 4c) was located about 20 km off the Mexican coast. SkinDeEP measurements were made from 14:01 to 15:24. Downwelling shortwave radiation had an

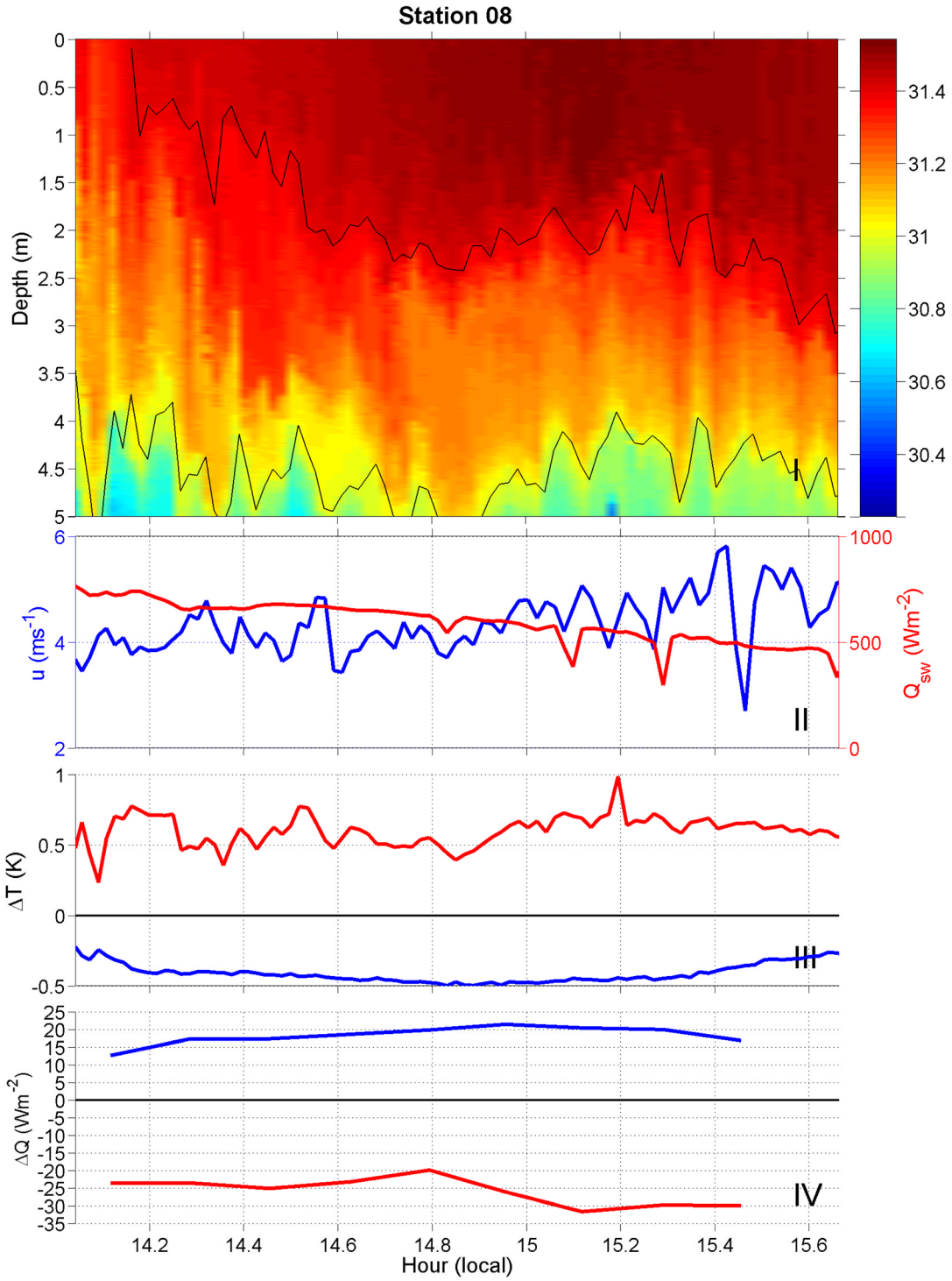

Figure 4d. Same as Figure 4a.

average value of 625 Wm^{-2}, with the peak insolation of 877 Wm^{-2} occurring at 12:17, some hours before the deployment. The average skin temperature was 30.8°C. Wind speeds reached a maximum of 6.6 ms^{-1}, with an average value of 5.4 ms^{-1}. There was about 0.6°C thermal stratification in the upper 2 m. The solid white line in the SkinDeEP plot is the minimum temperature between 2 m and 4 m, indicating a persistent cooler layer for the 70 min of the profile time series. It is likely that stabilization by reduced salinity was the result of fresh-water runoff, given the proximity of the coast. The solid black line is a single isotherm of 30.9°C.

[24] The ΔT_c and ΔT_{cw} had mean values of −0.25 and +0.24 K, respectively. There was a warm layer with a mean value of 0.5 K.

[25] The heat flux errors ΔQ_c and ΔQ_{cw} were almost symmetrical with mean values of +12.5 Wm^{-2} and −12 Wm^{-2}. The error associated with the warm layer

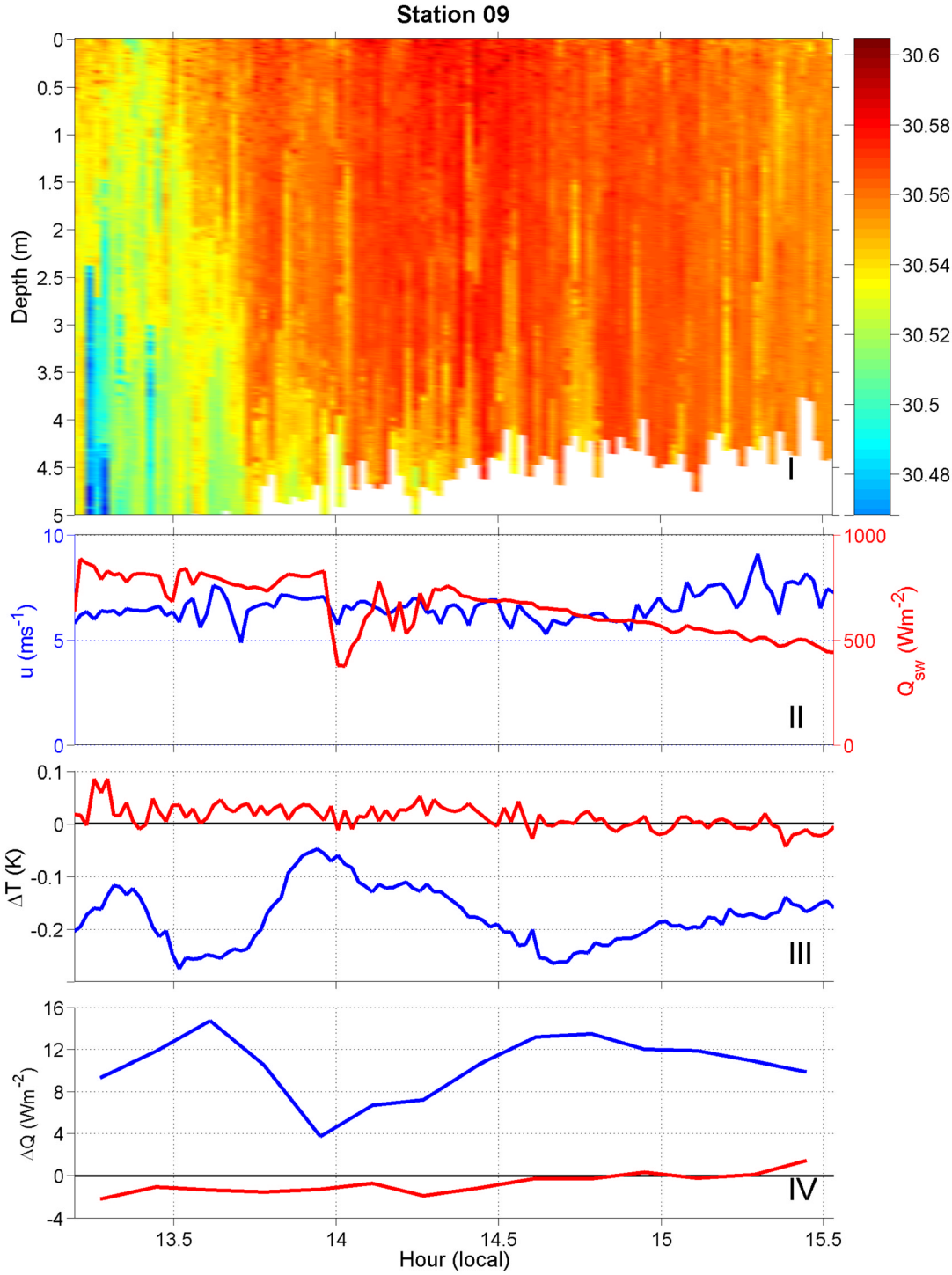

Figure 4e. Same as Figure 4a.

ΔQ_w was -24 Wm^{-2}. The latent heat flux was significantly larger than the longwave, followed by relatively small sensible heat fluxes (Table 3). The largest contributor to the heat loss error came from the latent heat flux.

3.4. Station 8

[26] The deployment at station 8 (Figure 4d) was in the same area as station 7, and was conducted at the same time of day, i.e., from about 14:00 to 15:40. The mean wind speed was 4.3 ms^{-1}, and briefly reached a maximum of 5.8 ms^{-1}. Insolation had an average value of 595 Wm^{-2}, from a maximum value of 720 Wm^{-2} at 11:12. The lower insolation compared to other days was due to cloud cover, which persisted for several hours. There was a warm layer of more than 1.2 K. There are two isotherms in the SkinDeEP plot: 31.4 and 31.0°C, the vertical displacements of which are in phase with each other. This is likely due to internal wave activity.

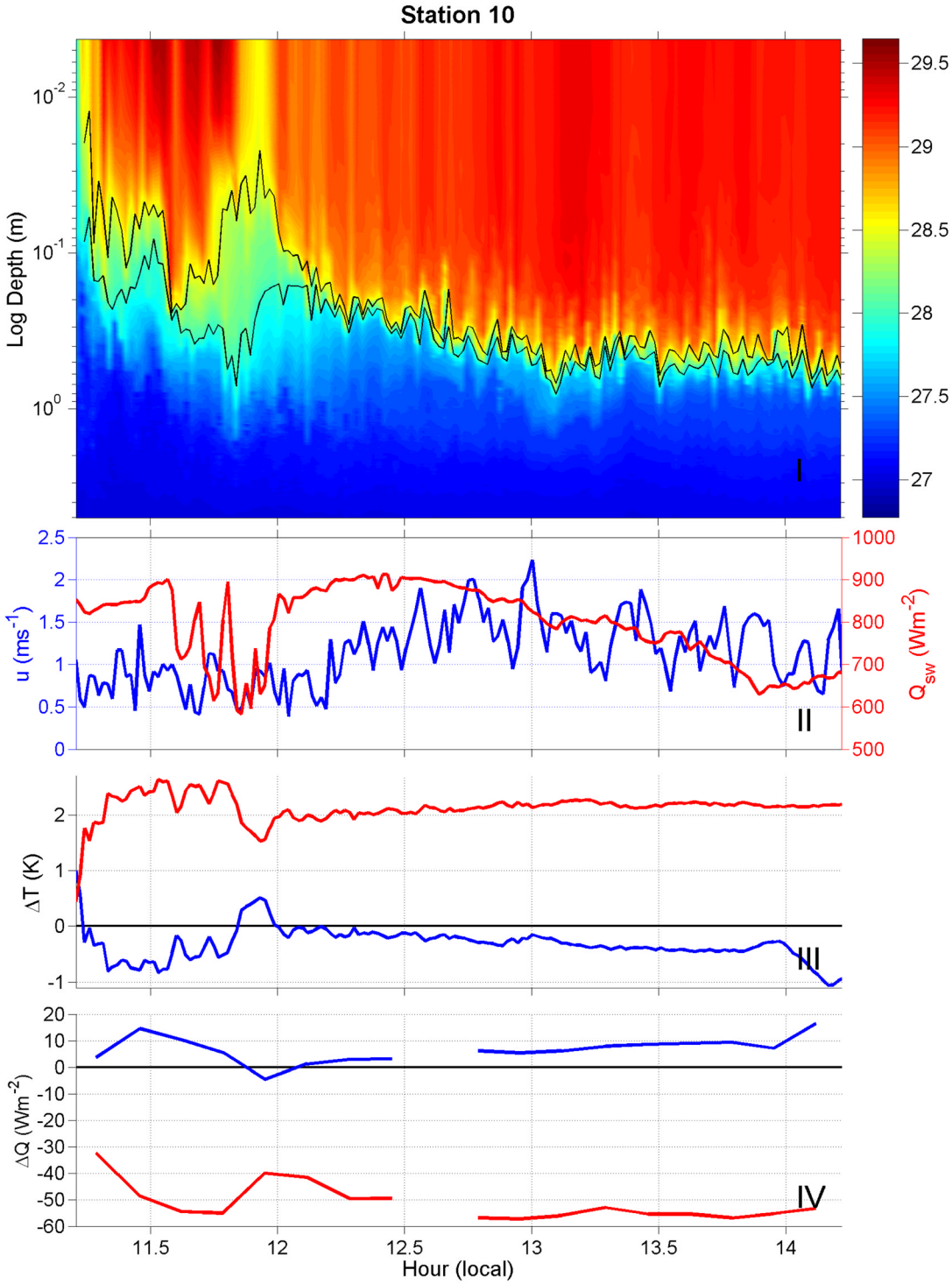

Figure 4f. Same as Figure 4a.

[27] The skin temperature was almost invariant, i.e., 31.1 ± 0.06°, and ΔT_c had a mean value of −0.41 K. There was considerable variability in the T_{5m} data, with a standard deviation of 0.1 K producing a positive ΔT_{cw} with a maximum value of +0.54 K. The warm layer had the largest temperature difference with a maximum value of +1 K.

[28] Heat loss to the atmosphere was dominated by evaporation, followed by longwave and sensible heat flux: ΔQ_c reached a maximum value of +21.4 Wm^{-2}, with a mean value of +18.3 Wm^{-2}; ΔQ_{cw} had a mean value of −7.5 Wm^{-2}. The warm layer resulted in a mean error of ΔQ_w = −25.7 Wm^{-2}.

3.5. Station 9

[29] Station 9 (Figure 4e) was located further north, about 323 km from station 8 (Figure 2 and Table 1). The wind

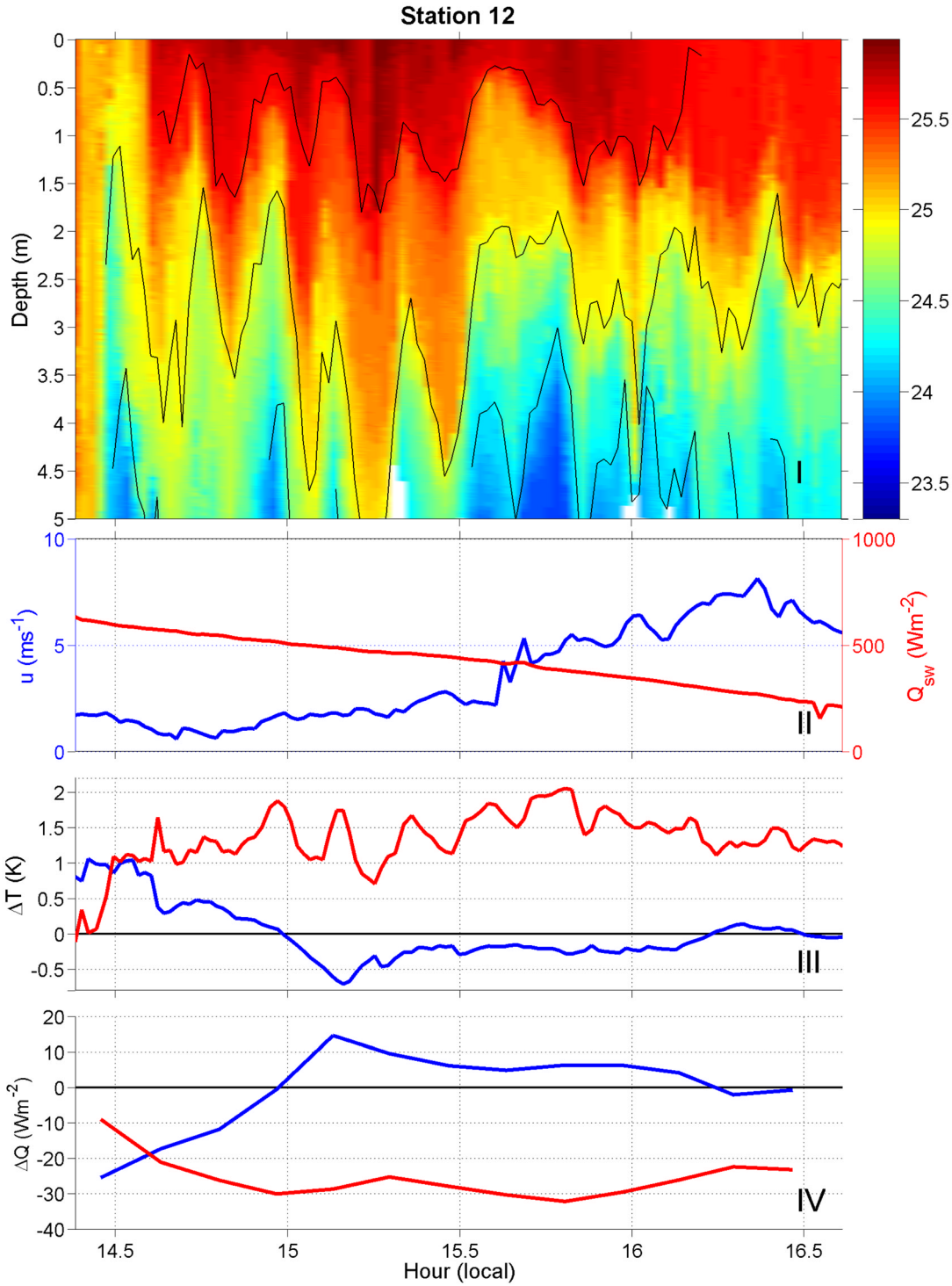

Figure 4g. Same as Figure 4a.

speed was quite steady from the north, with an average value of 6.6 ms^{-1} and a standard deviation of 0.7 ms^{-1}. The mean insolation was 654 Wm^{-2}, with a daily maximum of 890 Wm^{-2} at 12:18. The temperature range for the Skin-DeEP data was less than 0.2 K, indicating a well-mixed upper water column.

[30] The skin temperature varied by about 0.2 K during the measurement period. The homogeneous subsurface temperature field allowed for a depth-independent bulk measurement when deriving the ΔT values. The mean values for ΔT_c and ΔT_{cw} were −0.18 and −0.16 K, respectively. There was no warm layer, with a mean ΔT_w of 0.01 K.

[31] Station 9 had the largest heat flux out of the ocean, with latent heat fluxes of greater than 200 Wm^{-2} (Figure 3), associated with the relatively high winds. Heat flux errors

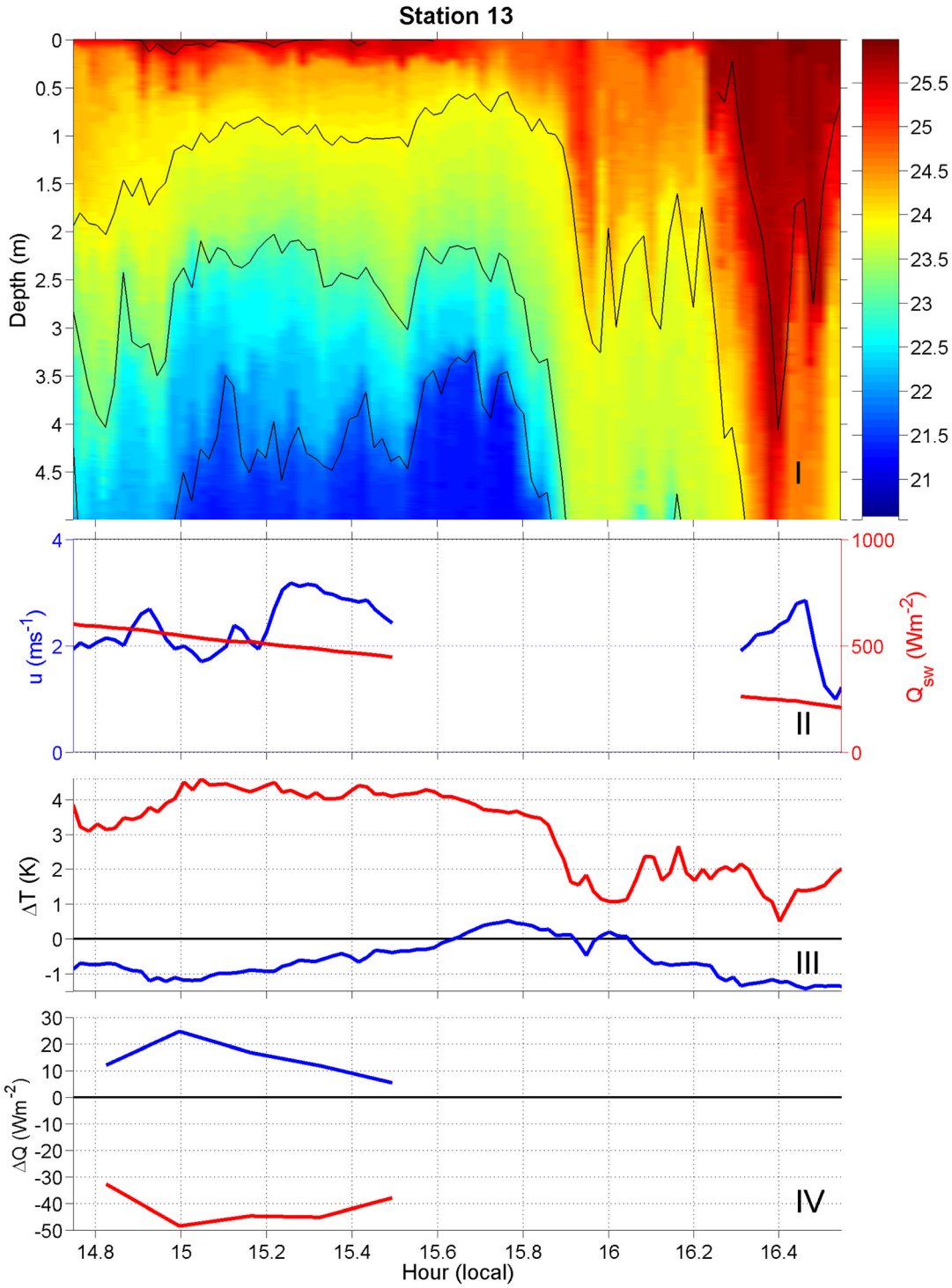

Figure 4h. Same as Figure 4a.

ΔQ_c and ΔQ_{cw} had mean values of +10.4 and +9.7 Wm^{-2}, respectively. The sensible and longwave errors were no more than +2 Wm^{-2}.

3.6. Station 10

[32] Figure 4f shows station 10, which was situated at the tip of the Baja Peninsula, and was the longest SkinDeEP deployment with 161 profiles. The measurements were made from 11:12 to 14:13. The mean wind speed was 1.1 ms^{-1}. The peak shortwave radiation was 912 Wm^{-2}, which occurred at 12:25. The SkinDeEP data are presented with a log scale for the depth, as practically no variability existed below 1 m. Within the upper meter, there was temperature stratification of up to 2.7 K. During this deployment, the warming was briefly interrupted by the passage of clouds, which caused the insolation to decrease

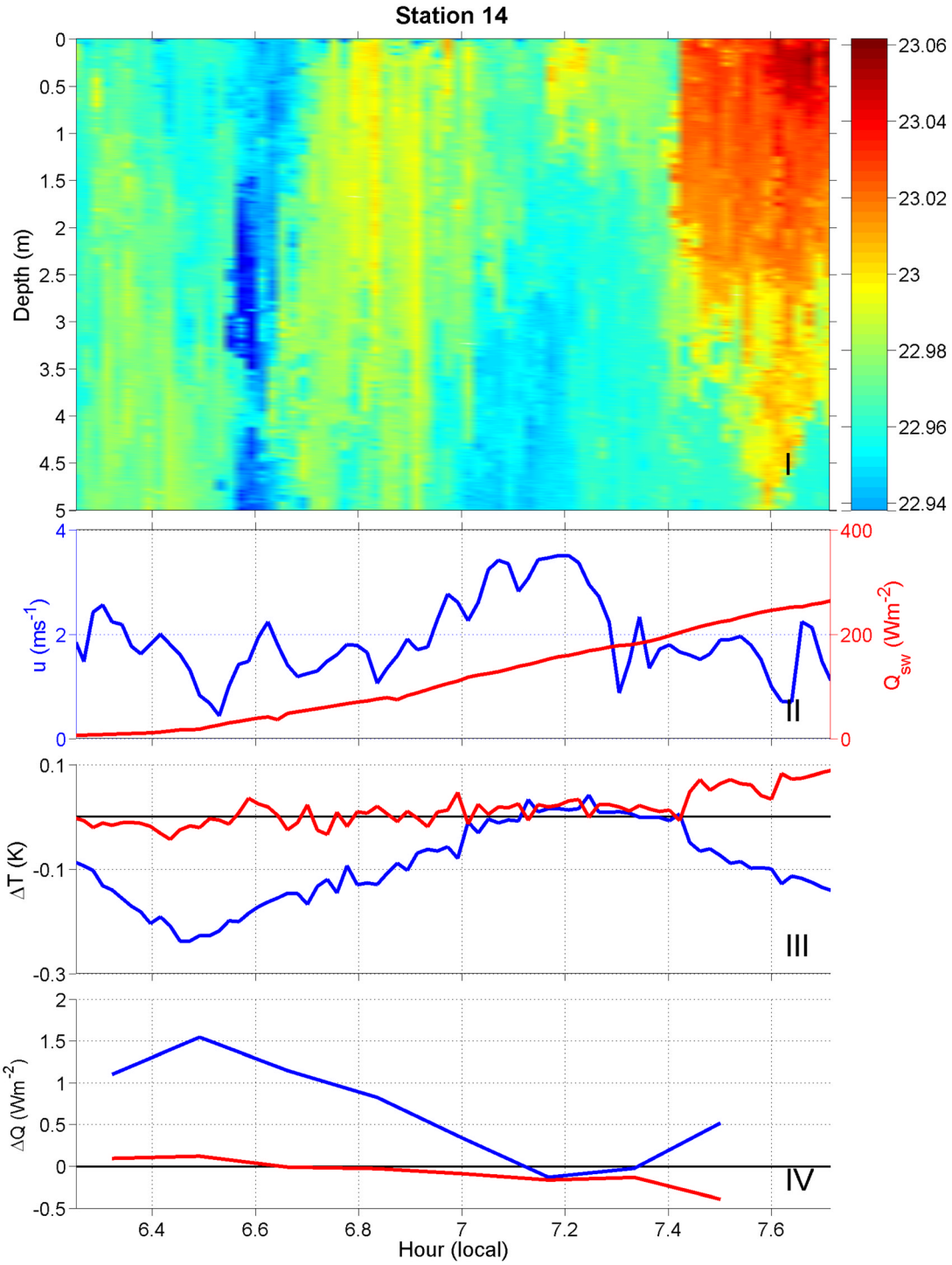

Figure 4i. Same as Figure 4a.

from 900 to 600 Wm^{-2} from about 11:30 to 12:00. The upper few decimeters responded to this drop in downwelling radiation, which is reflected in the SkinDeEP measurements. The warming recommenced after the Sun re-emerged from behind the cloud, and the stratification developed to a depth of about 0.6 m. There are two isotherms shown in the SkinDeEP subplot: 28 and 28.5°C, indicating the very strong gradient present at ~0.5 m.

[33] The ΔT_c had a mean value of −0.31 K, and ΔT_{cw} was +1.82 K. The ΔT_c data are predominantly negative, except for a short period around local noon, when the cloud passed overhead. The mean warm-layer temperature ΔT_w was 2.1 K.

[34] The errors resulting in the heat flux calculations were large: the maximum value for ΔQ_{cw} was −52 Wm^{-2}, and for Q_c it was +16 Wm^{-2}. ΔQ_w has the highest error with a maximum value of −57 Wm^{-2}. Although the absolute heat

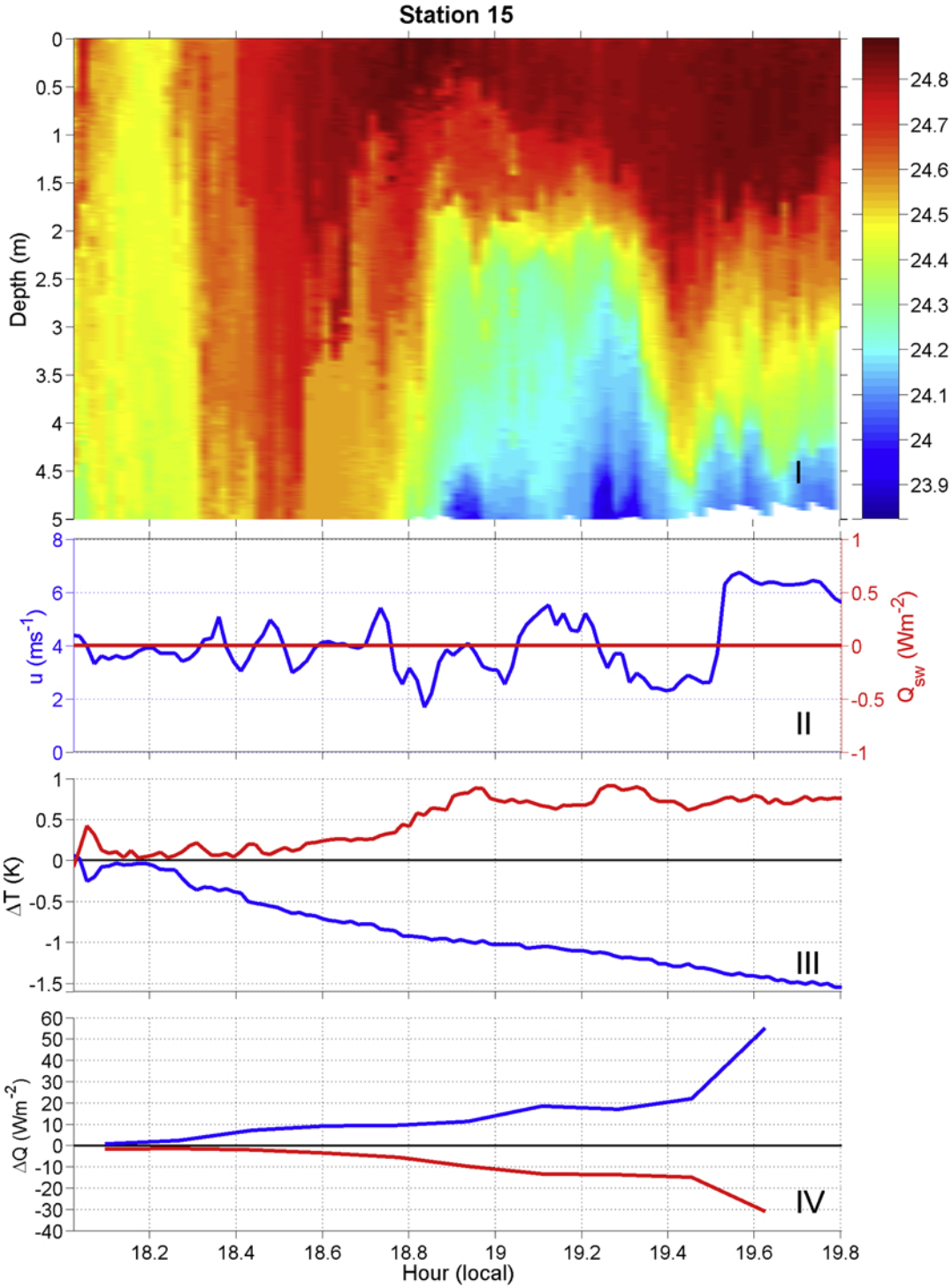

Figure 4j. Same as Figure 4a.

loss was dominated by the longwave flux (Table 3), the largest error was associated with the latent heat flux.

3.7. Station 12

[35] Station 12, presented in Figure 4g was located at the Midriff of the Gulf (Figure 2), and occurred from 14:22 to 16:37. The mean skin temperature was 24.9°C. There was a linear decrease in downwelling radiation from 630 to 150 Wm^{-2}, although the day was perfectly clear with maximum insolation of 860 Wm^{-2} at 11:30. The wind speed was initially below 3 ms^{-1}, but at 15:30 it increased to about 5 ms^{-1}, and reached a maximum of 8.1 ms^{-1} toward the end of the measurement period. The SkinDeEP profiles showed significant diurnal warming: the difference between the minimum and maximum SkinDeEP temperature was 2.4 K. Some cooling in the upper 1 m occurred from about 16:00, probably associated with the increase in wind speed. There is also significant variability in the

SkinDeEP data, suggesting internal wave activity. The three isotherms (24.2, 24.9, and 25.6°C) show very pronounced vertical displacements with a periodicity of about 5 cph during the first half of the station. The vertical displacements appear to be coherent with depth, with amplitudes diminishing toward the surface.

[36] There was considerable variability in the ΔT_{cw} and ΔT_w data, with standard deviations of 0.37 and 0.38 K, and mean values of 1.34 and 1.33 K, respectively. The ΔT_c had a mean value of 0.01 K, going from positive to negative during the deployment.

[37] The flux errors were once again dominated by the latent heat flux, even though the largest component of the absolute heat loss at the surface was through the net longwave, which was the highest during all the SkinDeEP deployments (Table 3). The maximum ΔQ_w, ΔQ_{cw} and ΔQ_c values were −32.1, −38.3 and +14.6 Wm^{-2}. The sensible heat flux error was negligible, but the longwave error contributed a mean value of −10 Wm^{-2} to ΔQ_w.

3.8. Station 13

[38] The measurements at station 13 are shown in Figure 4h. The deployment lasted just about 2 hours, from 14:44 to 16:34, and was again located in the Midriff of the Gulf. The wind speed did not exceed 3.2 ms^{-1} and the downwelling shortwave reached a maximum of 600 Wm^{-2}. The profile data showed the largest diurnal warming event on this cruise, which was at 15:02. The temperature at 5 m was 21.3°C, with a surface temperature at 25.9°C, i.e., a warm layer of 4.6 K. There are four isotherms shown in the SkinDeEP plot: 21.8, 23.1, 23.9, and 25.6°C. These isotherms do not vary greatly with depth until 15:50, at which point they plunge down with a cooling surface and a warming of the waters at depth. The 25.6°C isotherm has a stronger presence after 16:15, probably due to advection rather than shortwave absorption, as the insolation diminished to ∼200 Wm^{-2}.

[39] There were very large ΔT_w and ΔT_{cw} values, reaching maxima of >4 K each. There was a relatively small variance in T_{skin} during this deployment (standard deviation of 0.26°C), and the ΔT_c was mostly negative, except for a short period at 15:40, with a mean value of −0.6 K.

[40] Absolute heat loss was dominated by the large net longwave flux, with small values for sensible and latent fluxes. Largest errors were −48, −33 and +24 Wm^{-2} for ΔQ_w, ΔQ_{cw} and Q_c, respectively.

3.9. Station 14

[41] Station 14 (Figure 4i) was unique in that SkinDeEP was deployed just before sunrise at 06:15. Measurements were made for 1.5 hours while the Sun rose, with the shortwave radiation reaching 270 Wm^{-2} at the end of the measurement period. The wind speed reached a maximum of 3.5 ms^{-1} during the deployment. Station 14 was located in the same region as station 13, and no residual of the diurnal warming from the previous day was apparent. The temperature structure in the water was patchy, with a maximum difference of 0.1°C between the coldest and warmest patches. At 07:25, a warm patch of water appeared which coincided with the insolation reaching 200 Wm^{-2}, as well as a drop in wind speed from 3.5 ms^{-1} to about 1.5 ms^{-1}. The surface appeared to be quite sensitive to the conditions, and there was little delay between the drop in wind and the onset of warming.

[42] A cool skin existed throughout the deployment except for a brief period around 07:10 when both ΔT_c and ΔT_{cw} reached +0.04 K. ΔT_w was fairly constant during the deployment, except toward the end of the measurement period, when the ΔT records began to diverge due to the onset of stratification.

[43] There were very small fluxes of sensible and latent heat, and the errors from these heat loss components were negligible. The net longwave flux had a similar value to the previous station (Table 3), but the heat loss error was negligible at less than 2 Wm^{-2}.

3.10. Station 15

[44] Station 15 (Figure 4j) was again located in the Midriff of the Gulf. The deployment was on the same day as station 14, but after sunset. The R/V *Melville* followed SkinDeEP during this deployment, and maintained the instrument within 100 m from the starboard bow, directly within the field-of-view of the M-AERI. SkinDeEP measurements commenced at 18:00 and continued until 19:48. The wind speed had an average value of 4.1 with a standard deviation of 1.2 ms^{-1}.

[45] The ΔT_c data showed an almost linear decrease, due to the skin temperature decreasing from 24.5 to 23.3°C, indicating significant heat loss to the atmosphere. The $T_{subskin}$ data were fairly constant during this period, and so the change in ΔT_c was primarily as a result of the change in T_{skin}. The ΔT_c data had a mean value of −0.87 K. The ΔT_{cw} values were more variable due to the breakdown in stratification, and had a mean value of −0.39 K. There was a mean warm-layer temperature difference of +0.48 K.

[46] The heat loss error was fairly small, until 19:30, when ΔQ_c jumped from +14 Wm^{-2} to +46 Wm^{-2}. This coincided with a sharp increase in the wind speed from 3 ms^{-1} to 6.5 ms^{-1}. The increase in ΔQ_{cw} was smaller, with an increase from +7 Wm^{-2} to +24 Wm^{-2}. For ΔT_w, this resulted in a sharp increase from −14 to −30 Wm^{-2}. The error associated with the latent heat flux was the largest contributor to total heat loss error.

4. Discussion

[47] The measurements from SkinDeEP during the MOCE-5 cruise provide a detailed record of diurnal warming over several days and under a variety of conditions. Early in situ studies of diurnal warming were conducted by *Stommel et al.* [1969], who reported on observations of nine diurnal cycles, and demonstrated a good balance between insolation and the increase in heat storage in the upper 60 m of the ocean. *Stramma et al.* [1986] used both in situ and satellite measurements to investigate diurnal warming and found maximum day-night SSTs of 3.5 K, with good agreement between satellite and in situ measurements. *Soloviev and Lukas* [1997] made measurements of the diurnal thermocline with a free-rising profiler and bow-mounted probes. Vertical warming of more than 3 K in the upper 1 m and horizontal variability of about 2 K over 0.2–6 km was observed. More recently, *Gentemann et al.* [2003] analyzed satellite SSTs and found that under favorable conditions, diurnal warming can begin

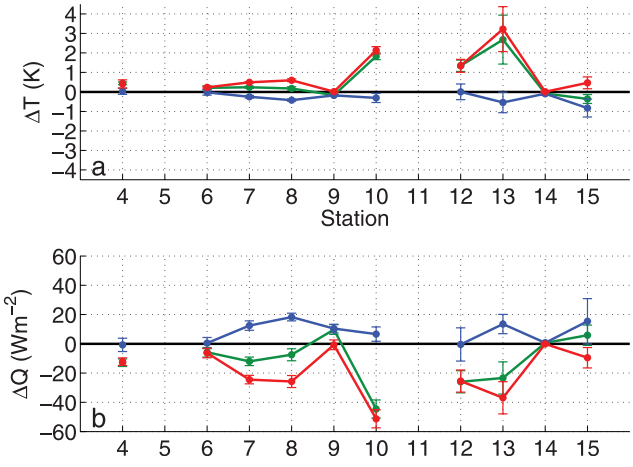

Figure 5. (a) Mean cool-skin temperature difference ΔT_c (blue); mean warm-layer temperature difference ΔT_w (red); ΔT_{cw} (green). (b) Mean heat loss errors (ΔQ) for the corresponding ΔT above. Error bars indicate one standard deviation about the mean.

at 8 AM and peak at 3 PM. An empirical model was derived from the SST and wind speeds which accounted for a significant part of the observed diurnal warming. *Stuart-Menteth et al.* [2003] analyzed ten years of NOAA AVHRR satellite-derived SST for global variations of diurnal warming by subtracting daily nighttime from adjacent daytime values. This study confirmed that diurnal warming is associated with conditions of low wind and high insolation. Other satellite observations have revealed large amplitude SST (up to 3 K) variability in relation to atmospheric convection in the Indian Ocean. *Duvel et al.* [2004] stressed the importance of air-sea fluxes in driving these SST anomalies. In a more recent study, J.-P. Duvel and J. Vialard (Indo-Pacific sea surface temperature perturbations associated with intraseasonal oscillations of the tropical convection, submitted to *Journal of Climate*, 2005) have shown that almost every winter (except in early 1998), this region was home to a strong cooling of SST, associated with very strong convective variability.

[48] Phytoplankton cause localized heating through increased attenuation of light. *Ramp et al.* [1991] observed temperature differences of up to 4.7 K between measurements at depths of 4 cm and 2 m. Coincident measurements of chlorophyll concentration were about 8 mg m^{-3}. Areas of lower chlorophyll showed less heating. *Kahru et al.* [1993] used satellite SST and in situ data to show increases in SST from surface accumulation of cyanobacteria. Both *Ramp et al.* [1991] and *Kahru et al.* [1993] concluded that biologically induced heating occurred at low wind speeds. However, it is in the absence of wind mixing that near-surface water optimally stratify, and so there is a complicated relationship between biological heating and mixing (or lack thereof). For example, the concentration of chlorophyll for the measurements during station 10 (Figure 4f) is 0.15 mg m^{-3}, and yet there was a warm layer of over 2.7 K. However, wind speed was minimal (Table 3). On the other hand, during station 8 (Figure 4d), the mean chlorophyll concentration was 5.5 mg m^{-3} with a maximum warm layer of 1.2 K, but the mean wind speed was 4.3 ms^{-1}.

[49] Figure 5 is a summary of ΔT and ΔQ, showing the mean values for each station. There were three stations where the absolute value of $|\Delta T_c|$ was greater than $|\Delta T_w|$. These were characterized by moderately high winds which led to a breakdown in stratification (station 9); predawn measurements where there was a "clean slate," i.e., no vestiges of stratification from the day before (station 14); and after sundown, where stratification breakdown occurred due to heat loss to the atmosphere (station 15). During the remaining stations, the warm-layer temperature difference ($|\Delta T_w|$) was greater, reaching 3 K during station 13. This was much larger than $|\Delta T_c|$, which reached an absolute maximum of 0.9 K during station 15.

[50] Heat flux uncertainties associated with the warm-layer temperature difference (ΔQ_w) are generally larger than those associated with the cool skin (Figure 5), except for the three cases mentioned above. The largest mean error of 51 Wm^{-2} occurred at station 10, which had the lowest wind speed and the highest stratification encountered. The contribution of the latent flux error was 66% of the overall error, followed by a net longwave error of 27%. The large errors in the heat flux calculations were directly related to the large differences in SST, and were not influenced by wind speed. Under higher winds, the increased mixing would result in a lower warm-layer temperature difference. For example, during station 9 (Figure 4e), there was no warm layer present due to the relatively high winds (Table 3), but the error from the cool skin was 10 Wm^{-2}. The results from this station display the sensitivity of the heat flux calculation to changes in water temperature; in this case, a 0.04°C difference between $T_{subskin}$ and T_{5m}, produced a 2.3 Wm^{-2} error in the total heat loss at the surface.

[51] There were two "nighttime" deployments: one before sunrise (station 14) and one after sunset (station 15). For the predawn deployment, there was an average cool skin of only 0.1 K, although some heat loss occurred through the longwave radiative flux. The corresponding heat loss errors were negligible. For the evening deployment, there was considerable heat loss to the atmosphere, and the heat flux error associated with the cool skin was larger than the warm-layer error. Many of the parameterizations for predicting ΔT [e.g., *Saunders*, 1967; *Hasse*, 1971; *Wick et al.*, 1996] are for nighttime situations only. The most commonly used determination for nighttime conditions are during periods when the solar insolation is zero, but the data from station 15 (Figure 4j) indicate that precautions must be taken when assuming a nighttime well-mixed water column.

[52] Wind speed affects ΔT_c through the net heat flux and turbulent mixing. Wind speed increases the net heat flux, and according to the available parameterizations [*Saunders*, 1967; *Soloviev and Schlüssel*, 1996; *Fairall et al.*, 1996a], this will increase the temperature difference. However, this also leads to an increase in turbulent mixing, which will serve to thin the skin layer and thereby decrease the resulting temperature difference [*Wick et al.*, 1996]. The relationship between ΔT and wind speed is shown in Figure 6, where the data were averaged over wind speed bins of 0.5 ms^{-1}. The ΔT_{cw} data show the effect of stratification, especially at low winds, where values reach >1.5 K. In contrast, the ΔT_c showed a predominantly cool skin. It is surprising to see that the ΔT_c and ΔT_{cw} data do not converge at the higher wind speeds. This may be an artifact

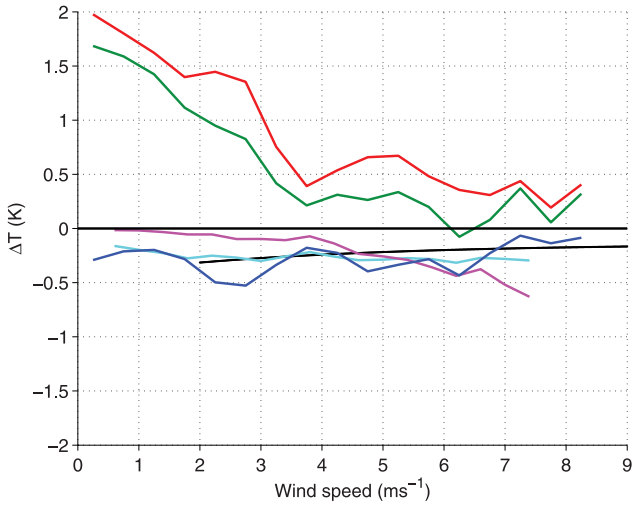

Figure 6. SkinDeEP skin-bulk temperature difference versus wind speed (bin averages) for ΔT_c (blue), ΔT_w (red), and ΔT_{cw} (green). Also shown is the parameterized relationships after *Donlon et al.* [2002] (black), *Fairall et al.* [1996a] (cyan), and *Soloviev and Schlüssel* [1996] (magenta). These parameterizations predict only the temperature difference across the conductive boundary layer ΔT_c. The latter two include a shortwave absorption parameterization, whereas *Donlon et al.* [2002] is purely empirical and was determined with nighttime data only.

and can probably be attributed to the measurements at stations 12, where there was increased variability in both the wind speed and ΔT data.

[53] Also plotted in Figure 6 are three parameterizations for the skin-bulk temperature difference, bin-averaged over 0.5 ms^{-1} bin sizes. The relationship after *Donlon et al.* [2002] (DON) is given by: $\Delta T = -0.14 - 0.3 \exp(-u/3.7)$. This expression is an empirical fit to several nighttime data sets where radiometric skin temperature data were available, and was considered to be unsuitable for winds below 2 ms^{-1}. *Fairall et al.* [1996a] (FAI) used the *Saunders* [1967] relationship, which was an argument based on dimensional analysis given by $\Delta T = \lambda \nu Q / k u_*$, where ν is the kinematic viscosity, and k is the thermal conductivity. *Fairall et al.* [1996a] developed an expression for λ which incorporated the transition from the free convection to a shear-driven regime at ~4 ms^{-1}. The parameterization from *Soloviev and Schlüssel* [1996] (SS) assumes that ΔT_c can be derived from a knowledge of the surface cooling, and absorption of shortwave radiation across the conductive boundary layer.

[54] For both the FAI and SS parameterizations, the ΔT increases with wind (Figure 6). This would indicate that the heat flux term, which will increase with wind, is causing the increase in the ΔT. However, the DON parameterization decreases from −0.3 K at 2 ms^{-1} to −0.17 K at 9 ms^{-1}. There is no clear trend with the ΔT_c data, although it has a tendency to decrease as the wind speeds increase. The SS parameterization exhibits a change in the rate of increase in ΔT at ~4 ms^{-1}, which could be related to the change in free to forced convection suggested by *Fairall et al.* [1996a] (although the FAI parameterization in Figure 6 does not exhibit a transition at this wind speed). *Veron and Melville* [2001] suggest that small-scale Langmuir circulations may be responsible for this change, as they observed the onset of Langmuir circulation to occur at wind speeds above ~3 ms^{-1}.

5. Conclusions

[55] Results from the SkinDeEP profiler have been presented, which was deployed in the Gulf of California during the MOCE-5 campaign. Profiles were made over a depth of 5 m, at an interval of about 1 minute. Simultaneous measurements from the M-AERI provided high-accuracy skin temperature data. SkinDeEP was deployed mostly in the early afternoon, its schedule dictated by shipboard logistics. Generally the conditions included low wind and high insolation.

[56] One of the obvious results from this study is the depth dependency of the ΔT during daytime. The ΔT_c data show that the skin temperature is normally cooler than the bulk ($T_{subskin}$ in this case). This would indicate that the amount of shortwave radiation absorbed within the conductive boundary layer is insufficient to overcome the cooling from the sensible, latent, and longwave heat fluxes, which act immediately at the ocean-atmosphere interface. This result agrees with *Wick et al.* [2005], who uses an improved shortwave absorption parameterization after *Ohlmann and Siegel* [2000] which resulted in the reduction of previous overestimates of diurnal skin layer warming. On the other hand, the ΔT_{cw} (i.e., the "conventional" skin-bulk temperature difference) reflects a skin temperature that is usually warmer than the 5 m bulk temperature.

[57] There can be no argument that the skin temperature is the most physically appropriate SST for calculating air-sea heat fluxes. However, often the only available SST during a shipboard campaign is the temperature from the TSG, and in these situations, this is used for the calculation of the air-sea heat fluxes. This study has quantified the errors in the heat flux components for both the cool-skin and the warm layer. Figure 7 emphasizes the relative contributions from both effects, with the warm layer resulting in a larger error than the cool skin. There is considerable scatter in Figure 7, but

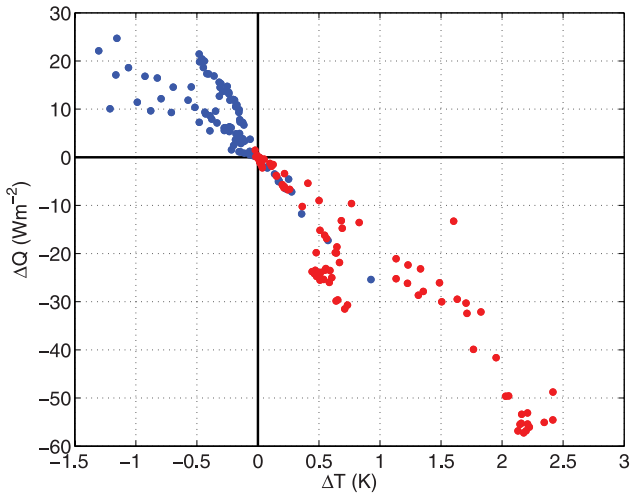

Figure 7. Relationship between ΔT and ΔQ for warm-layer (red) and cool-skin (blue). The data are averaged over 10 min. Note that one cool-skin data point at ~55 Wm^{-2} (during station 15; section 3.10; Figure 4j) is not shown.

for a ΔT_c or ΔT_w of 0.5 K, the resulting heat flux errors are up to 20 and 30 Wm^{-2}, respectively.

[58] The results here provide an argument for routine radiometric measurements. When radiometric measurements are not available, models must be used. However, most ΔT parameterizations require that the net heat flux be known a priori. The DON relationship could be used for high wind cases, where a constant offset of −0.17 K can be added to the bulk temperature, with the assumption that the surface waters are well mixed and T_{depth} is equivalent to $T_{subskin}$. Under low wind, daytime conditions, it would be necessary to eliminate the effect of stratification by employing a model such as *Fairall et al.* [1996a] or *Jenkins and Ward* [2005].

[59] Nighttime parameterizations are appropriate under daytime conditions if a measurement of $T_{subskin}$ is available (i.e., FAI and SS). This would be impossible to obtain as an underway measurement, as it would require maintaining a thermometer at the ocean surface from a moving vessel (indeed it is difficult to obtain a SST measurement with the TSG which is completely free of the ship's influence). Short-term deployments of SkinDeEP can provide an insight into the behavior of ΔT during conditions amenable to thermal stratification. For example, *Ward et al.* [2004a] have presented results from a cruise in the Mediterranean where SkinDeEP remained within the field-of-view of M-AERI for three separate deployments, two of which captured a complete diurnal cycle.

[60] Further studies are required to understand the effect of biology on stratification in the near-surface layer, and if the concentration of chlorophyll can attenuate the effects of mixing.

[61] Under conditions of daytime low wind, the warm layer will dominate the heat flux error, driven by the differences in temperature across the diurnal thermocline. Under high wind conditions, where the absolute latent and sensible heat fluxes will be elevated, the heat flux error associated with the cool skin will dominate. Heat flux errors associated with the warm layer will be of $O(10-50)$ Wm^{-2}, whereas errors associated with the cool skin will approach $O(1-10)$ Wm^{-2}.

[62] **Acknowledgments.** The author would like to thank Peter Minnett for the opportunity to participate in the MOCE-5 cruise, and for providing the M-AERI skin temperature data. Thanks also to Denis Clark for the assistance and support for the SkinDeEP deployments. The cooperation of captain, crew, and colleagues aboard the R/V *Melville* was invaluable. The Matlab code for Figure 2 was supplied by Stephanie Flora (MLML). The development of SkinDeEP was funded through the Research Council of Norway (Prosjektnr. 127872/720). Support was provided by the European Commission under the Marie Curie Fellowship contract ERBFMBICT983162. Further support was provided by NSF grant OCE-0241834 and National Oceanographic Partnership Program Award NNG04GM56G. This is WHOI contribution 11228.

References

Donlon, C. J., P. J. Minnett, C. Gentemann, T. J. Nightingale, I. J. Barton, B. Ward, and J. Murray (2002), Toward improved validation of satellite sea surface skin temperature measurements for climate research, *J. Clim.*, *15*, 353–369.

Duvel, J.-P., R. Roca, and J. Vialard (2004), Ocean mixed layer temperature variations induced by intraseasonal convective perturbations over the indian ocean, *J. Atmos. Sci.*, *61*, 1004–1023.

Fairall, C. W., E. F. Bradley, J. S. Godfrey, G. A. Wick, J. B. Edson, and G. S. Young (1996a), Cool-skin and warm-layer effects on sea surface temperature, *J. Geophys. Res.*, *101*, 1295–1308.

Fairall, C. W., E. F. Bradley, D. P. Rogers, J. B. Edson, and G. S. Young (1996b), Bulk parameterization of air-sea fluxes for tropical ocean-global atmosphere coupled-ocean atmosphere response experiment, *J. Geophys. Res.*, *101*, 3747–3764.

Gentemann, C. L., C. J. Donlon, A. Stuart-Menteth, and F. Wentz (2003), Diurnal signals in satellite sea surface temperature measurements, *Geophys. Res. Lett.*, *30*(3), 1140, doi:10.1029/2002GL016291.

Gregg, M. C., and T. B. Meagher (1980), The dynamic response of glass-rod thermistors, *J. Geophys. Res.*, *85*, 2779–2786.

Hasse, L. (1971), The sea surface temperature deviation and the heat flow at the air-sea interface, *Boundary Layer Meteorol.*, *1*, 368–379.

Jenkins, A. D., and B. Ward (2005), A simple model for the short-time evolution of near-surface current and temperature profiles, *Deep Sea Res.*, *52*, 1202–1214.

Kahru, M., J.-M. Leppänen, and O. Rud (1993), Cyanobacterial blooms cause heating of the sea surface, *Mar. Ecol. Prog. Ser.*, *101*, 1–7.

Minnett, P. J., and B. Ward (2000), Measurements of near-surface ocean temperature variability—Consequences on the validation of AATSR on ENVISAT, paper presented at ERS-ENVISAT Symposium "Looking Down to Earth in the New Millenium," Eur. Space Agency, Noordwijk, Netherlands.

Minnett, P. J., R. O. Knuteson, F. A. Best, B. J. Osborne, J. A. Hanafin, and O. B. Brown (2001), The marine-atmospheric emitted radiance interferometer (M-AERI), a high-accuracy, sea-going infrared spectroradiometer, *J. Atmos. Ocean. Technol.*, *18*, 994–1013.

Ohlmann, J. C., and D. A. Siegel (2000), Ocean radiant heating. Part II: Parameterizing solar radiation transmission through the upper ocean, *J. Phys. Oceanogr.*, *30*, 1849–1865.

Pawlowicz, R., R. Beardsley, S. Lentz, E. Dever, and A. Anis (2001), Software simplifies air-sea data estimates, *Eos Trans. AGU*, *82*(1), 2.

Ramp, S. R., R. W. Garwood, C. O. Davis, and R. L. Snow (1991), Surface heating and patchiness in the coastal ocean off central California during a wind relaxation event, *J. Geophys. Res.*, *96*, 14,947–14,957.

Saunders, P. (1967), The temperature at the ocean-air interface, *J. Atmos. Sci.*, *24*, 269–273.

Soloviev, A., and R. Lukas (1997), Observations of large diurnal warming events in the near-surface layer of the western equatorial Pacific warm pool, *Deep Sea Res.*, *44*, 1055–1076.

Soloviev, A., and P. Schlüssel (1996), Evolution of cool skin and direct air-sea gas transfer coefficient during daytime, *Boundary Layer Meteorol.*, *77*, 45–68.

Stommel, H., K. Saunders, W. Simmons, and J. Cooper (1969), Observations of the diurnal thermocline, *Deep Sea Res.*, *16*, 269–284.

Stramma, L., P. Cornillon, R. A. Weller, J. F. Price, and M. G. Briscoe (1986), Large diurnal sea surface temperature variability: Satellite and in situ measurements, *J. Phys. Oceanogr.*, *16*, 827–837.

Stuart-Menteth, A. C., I. S. Robinson, and P. G. Challenor (2003), A global study of diurnal warming using satellite-derived sea surface temperature, *J. Geophys. Res.*, *108*(C5), 3155, doi:10.1029/2002JC001534.

Veron, F., and W. K. Melville (2001), Experiments on the stability and transition of wind-driven water surfaces, *J. Fluid Mech.*, *446*, 25–65, doi:10.1017/S0022112001005638.

Ward, B., and P. J. Minnett (2002), An autonomous profiler for near surface temperature measurements, in *Gas Transfer at Water Surfaces*, *Geophys. Monogr. Ser.*, vol. 127, edited by M. A. Donelan et al., pp. 167–172, AGU, Washington, D. C.

Ward, B., P. Strutton, P. J. Minnett, I. Nardello, and L. Lazzara (2004a), Study of near surface radiant heating from irradiance and temperature profiles in the Mediterranean, in *Eos Trans. AGU*, *84*(52), Ocean Sci. Meet. Suppl., abstract OS 21C-02.

Ward, B., R. Wanninkhof, W. R. McGillis, A. T. Jessup, M. D. DeGrandpre, J. E. Hare, and J. B. Edson (2004b), Biases in the air-sea flux of CO_2 resulting from ocean surface temperature gradients, *J. Geophys. Res.*, *109*, C08S08, doi:10.1029/2003JC001800.

Ward, B., R. Wanninkhof, P. J. Minnett, and M. Head (2004c), SkinDeEP: A profiling instrument for upper decameter sea surface measurements, *J. Atmos. Ocean. Technol.*, *21*, 207–222.

Wick, G. A., W. J. Emery, L. H. Kantha, and P. Schlüssel (1996), The behavior of the bulk-skin sea surface temperature difference under varying wind speed and heat flux, *J. Phys. Oceanogr.*, *26*, 1969–1988.

Wick, G. A., J. C. Ohlmann, C. W. Fairall, and A. T. Jessup (2005), Improved oceanic cool skin corrections using a refined solar penetration model, *J. Phys. Oceanogr.*, *35*, 1986–1996.

B. Ward, Department of Applied Ocean Physics and Engineering, Woods Hole Oceanographic Institution, WHOI MS 12, Woods Hole, MA 02543, USA. (bward@whoi.edu)